Appendix A

Absorption Measurements for Hydrocarbon Fuel

This appendix gives the details of the technique used to measure the direct absorption of laser light at 3.39 μm by the C-H bond present in hydrocarbon fuels.

A.1 Direct Absorption Measurements

When a beam of collimated light of a specific wavelength, e.g. from a laser, passes through an absorbing medium, the molecules may absorb photons at that wavelength. Consequently, if the intensity of photons is measured before and after the medium, the change is proportional to the initial intensity of light, I_0, the path length, dx, and the absorption coefficient of the absorbing species, $\alpha(\nu)$:

$$I + dI = I - \alpha(\nu)I dx \tag{A.1}$$

$$\frac{dI}{I} = -\alpha(\nu)dx \ . \tag{A.2}$$

Integrating over the entire absorption path gives:

$$I = I_0 \exp\left[-\alpha(\nu)(x - x_0)\right] \tag{A.3}$$

The absorption coefficient $\alpha(\nu)$ is equal to the product of the molar density n and the absorption cross section σ_ν:
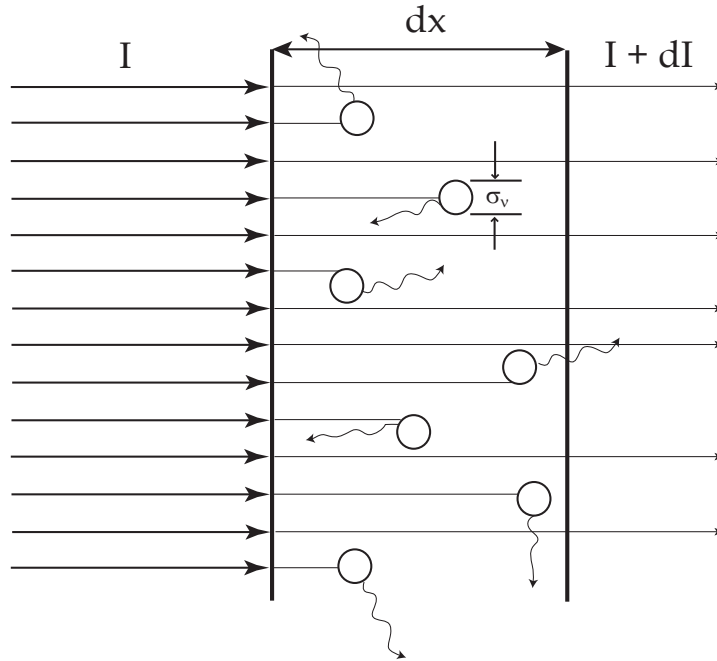
$$\alpha(\nu) = \sigma_\nu n \ . \tag{A.4}$$

Figure A.1: Beer's law diagram

Assuming the perfect gas law:

$$P = n\tilde{R}T \tag{A.5}$$

$$\alpha(\nu) = \sigma_\nu \frac{P}{\tilde{R}T} \ . \tag{A.6}$$

Let $L = (x - x_0)$ be the distance the laser light travels through the absorbing medium, giving the following form for Beer's law:

$$\frac{I}{I_0} = \exp\left(-\frac{\sigma_\nu P L}{\tilde{R}T}\right) \ . \tag{A.7}$$

In order to monitor the power variations of the laser over time the beam is split before it enters the test cell

$$I = I_1 + I_2$$

where I_1 is the reference beam and I_2 passes through the test cell as shown in Figure A.2. Now the necessary expressions can be written for the calibration of the absorption cross section, σ_ν, and calculating the partial pressure of fuel, P_{fuel}, where $I_1{}^0$ and $I_2{}^0$ are measurements taken when the

cell is evacuated

$$\sigma_\nu = \frac{\tilde{R}T}{P_{fuel}L} \left[\ln\left(\frac{I_1(t)}{I_2(t)}\right) - \ln\left(\frac{I_1{}^0}{I_2{}^0}\right) \right] \tag{A.8}$$

$$P_{fuel} = \frac{\tilde{R}T}{\sigma_\nu L} \left[\ln\left(\frac{I_1(t)}{I_2(t)}\right) - \ln\left(\frac{I_1{}^0}{I_2{}^0}\right) \right] . \tag{A.9}$$

Using the equations above, we can first estimate to what accuracy the absorption cross section can be measured and then predict the accuracy of the pressure measurement using this technique. The propagation of uncertainties for the absorption cross section is given by the following equation

$$\frac{d\sigma_\nu}{\sigma_\nu} = \frac{dT}{T} + \frac{dP}{P} + \frac{dL}{L} + \frac{d\Upsilon}{\Upsilon} , \tag{A.10}$$

where

$$\Upsilon = \left[\ln\left(\frac{I_1(t)}{I_2(t)}\right) - \ln\left(\frac{I_1{}^0}{I_2{}^0}\right) \right] . \tag{A.11}$$

Summing all the uncertainties given in Table A.1 results in a total uncertainty of 2.7%, given the absorption cross section of 38 $\pm$1 m^2/kmol. Using the same scheme we can compute the uncertainty in the fuel pressure, which is 5.2% of the measured value.

Table A.1: Uncertainty in fuel concentration measurements

	(x)	d(x)	units
T	295	1	K
P	10	.01	kPa
L	90	2	mm
Υ	0.373	3.45E-04	-

In this work a 3.39 μm wavelength HeNe laser is used to provide the collimated laser light (ThorLabs: H339P2) and passed through an optical chopper (Stanford Research System: SRS 540) running at 300 Hz allowing the detectors to relax and avoid saturation. The detectors used in this setup were two PbSe detectors manufactured by Judson Technology (Part Number: PE–0–53) that can be used at room temperature without cooling, and are sensitive in the infrared spectrum as shown in Figure A.3. The detector output was amplified using the circuit shown in Figure A.4

The wavelength of the absorption band is at 3.39 μm so that the test cell windows must transmit at this frequency. Sapphire was chosen as the window material, which transmits for wavelengths as long as 5 μm. The windows were connected to the Pyrex body of the vessel via Schott specialty glass and iridium glass (manufactured by M&M Glassblowing in Nashua, NH and the Caltech Glass
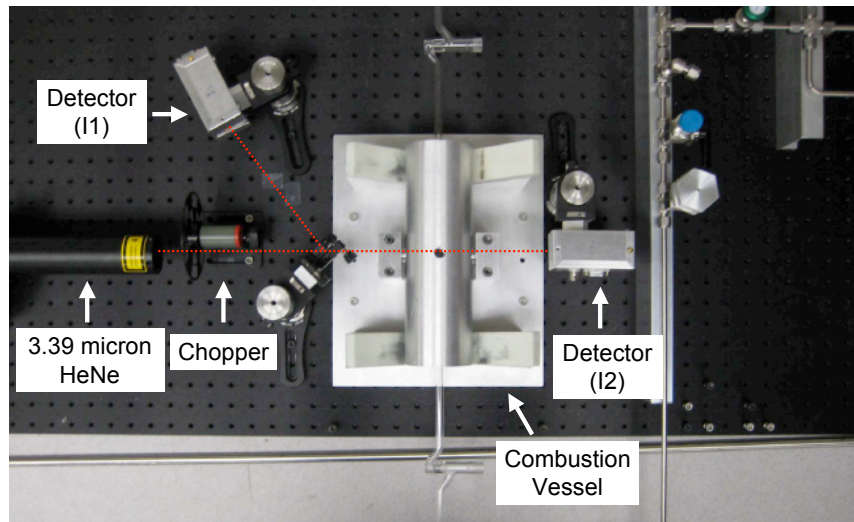
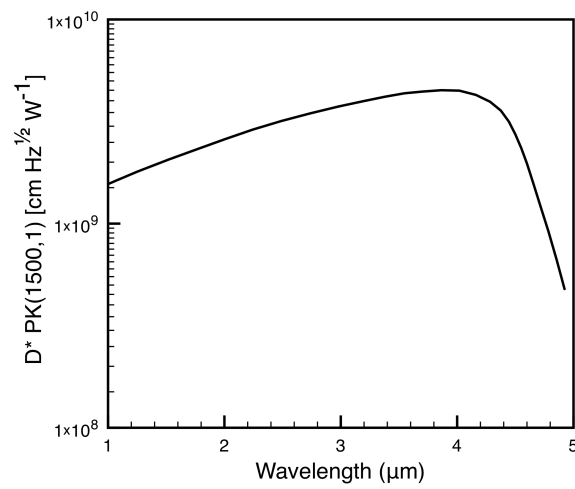Figure A.2: Fuel detection experimental setup

Figure A.3: Judson PE-0-53 detector sensitivity as function of wavelength (Teledyne Judson Technologies, 2000)
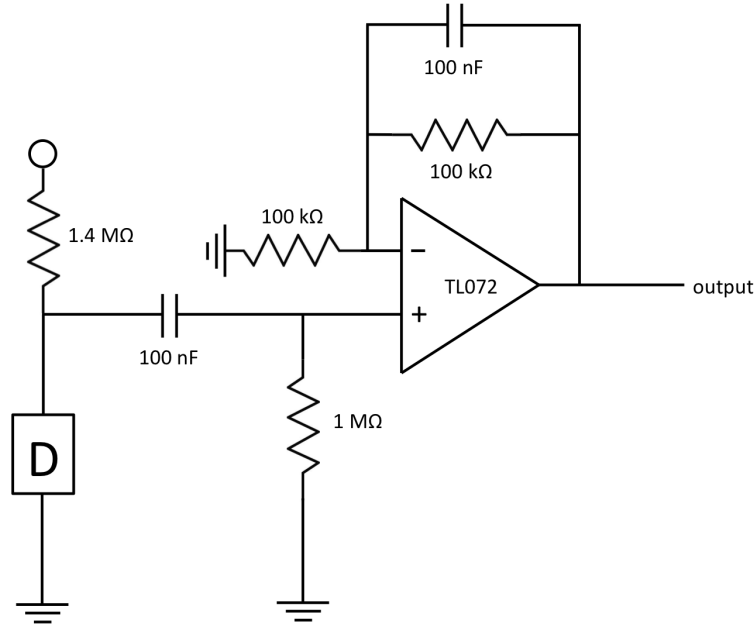
Figure A.4: Circuit used to amplify the signal from the detector (D)

Shop). In addition to using special windows, gold mirrors (ThorLabs: PF10-03-M01) were used for the beam steering due to their higher reflectance in the infrared.

LabView is used for data data acquisition and the program records continuous sets of 2000 samples at 50 kHz. This data is then directly analyzed and averaged giving an effective rate of 8 Hz during heating and slow reactions generating approximately 15k data points. Further, a second data acquisition board is triggered during an ignition event recording raw data at 150 kHz for a total of 200k data points. The maximum sampling rate for the optical fuel measurement is limited by the chopping frequency.

A sample set of raw data for the fuel measurements is shown in Figure A.5. For the fuel measurement, the intensity of the laser light going through the test cell, I_1, the intensity of the reference beam, I_2, and the synchronization output from the optical chopper (SYNC) are sampled at 50 kHz. The SYNC output, which is a 5 V square wave at the same frequency as the chopper, is used the trigger for the LabView script to begin recording 2000 samples. The processed chopper signal (SYNC > 2.5 V) is shown Figure A.5 as "Chopper (logic)", and then a subset as indicated by "Chopper (adjusted, logic)" is selected. The signals for I_1 and I_2, and the time are averaged in each selected window and thus give one data point for each window in which the chopper is "on".
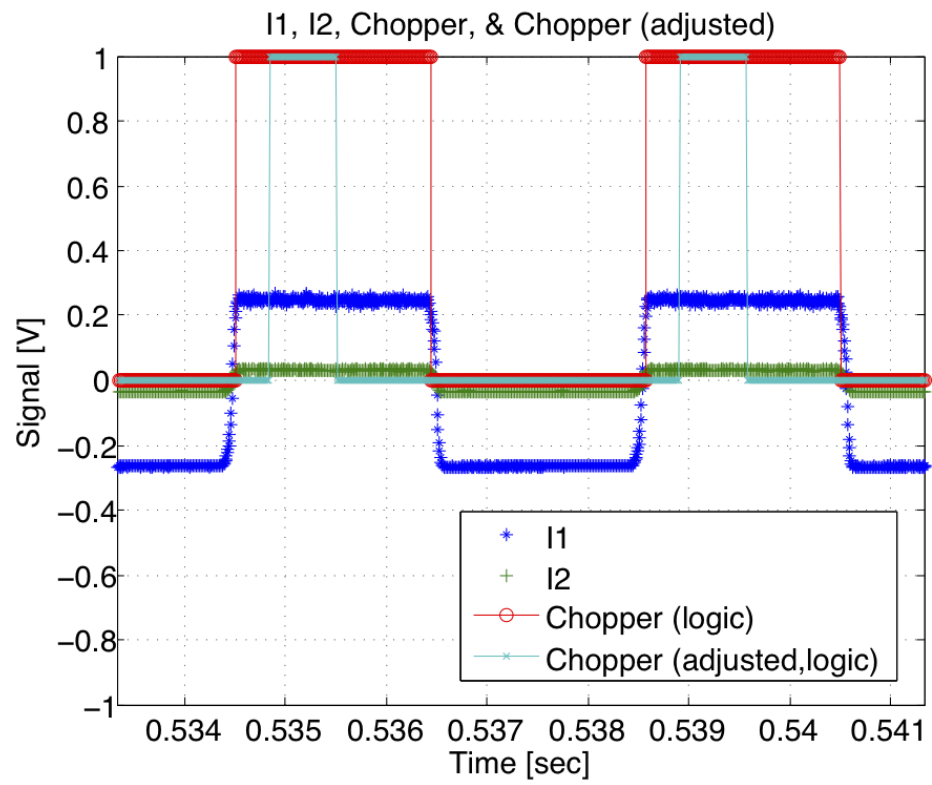
Figure A.5: Raw fuel data from shot 19

A.2 Absorption Cross Sections

As a reference the absorption cross sections at $\lambda = 3.39\,\mu$m for various hydrocarbons including n-hexane are given in Table A.2. Further measurements of absorption cross sections have been performed by Mével et al. (2012).

Table A.2: Absorption cross sections expanded from Klingbeil et al. (2006)

Hydrocarbon	Reference	Total Pressure [Torr]	σ_ν [m^{2}mole^{-1}]	Uncertainty [%]	Technique
Methane	Klingbeil et al. (2006)	760	21.1	3	HeNe
CH$_4$	Yoshiyama et al. (1996)	760	25.3	N/A	HeNe
	Tomita et al. (2003)	760	21.9	2	HeNe
	Perrin and Hartmann (1989)	760	22.5	5	HeNe
	Rothman et al. (2005)	760	21.4	N/A	Calculation
	Jaynes and Beam (1969)	30.4	36.7	N/A	HeNe
	Sharpe et al. (2004)	760	19.5	3	FTIR
Ethylene	Klingbeil et al. (2006)	760	0.459	3.5	HeNe
C$_2$H$_4$	Rothman et al. (2005)	760	0.386	N/A	Calculation
	Sharpe et al. (2004)	760	0.426	3	FTIR
	Hinckley and Dean (2005)	760	0.391	2	HeNe
Propane	Klingbeil et al. (2006)	760	20.2	3.4	HeNe
C$_3$H$_8$	Sharpe et al. (2004)	760	21.2	3	FTIR
	Tsuboi et al. (1985)	760	20.7	20	HeNe
	Yoshiyama et al. (1996)	760	23.9	N/A	HeNe
	Jaynes and Beam (1969)	760	48.9	N/A	HeNe
	Jaynes and Beam (1969)	23	20.3	N/A	HeNe
Hexane	Jaynes and Beam (1969)	11.4	45	N/A	HeNe
C$_6$H$_{14}$	Drallmeier (2003)	650	38.5	5	HeNe
	This Work	760	38	2.6	HeNe

N/A - not available

This page intentionally left blank.

Appendix B

Second Harmonic Detection of Oxygen with Tunable Diode Lasers

The following section gives the details for second harmonic detection of oxygen concentration that lead to Equation 2.4 in Section 2.2.3. The analysis of second harmonic detection described here was derived by Reid and Labrie (1981). In order to detect weak absorption features a tunable diode laser is modulated at a high frequency, while the mean wavelength of the laser is scanned more slowly across the feature. The intensity only drops very slightly as the wavelength reaches the wavelength at which the molecules absorb the photons. The change of the wavelength must be accounted for in the Beer-Lambert law and is written here in terms of the frequency of light $\nu = c/\lambda$, where λ is the wavelength and c is the speed of light:

$$I(\nu) = I_0(\nu) \exp\left(-\alpha(\nu)L\right) \tag{B.1}$$

Assuming that the absorption lines are weak $\alpha(\nu)L < 0.05$, the following approximation is valid:

$$I(\nu) \simeq I_0(\nu) \left[1 - \alpha(\nu)L\right] \tag{B.2}$$

In order to obtain a harmonic output, the electrical current input to the laser diode is modulated at a specified frequency, ω, which in turn modulates the wavelength of light emitted by the laser diode:

$$\nu(t) = \bar{\nu} + a\cos(\omega t) \tag{B.3}$$

The mean frequency, $\bar{\nu}$, is ramped slowly (80 Hz) relative to the modulation, ω, (23.5 kHz). For small ramping amplitude the incident light intensity is constant:

$$I(\nu) \approx I_0(\nu_0) \approx I_0 \tag{B.4}$$

Now the received intensity at the detector can be written as:

$$I(\nu) = I_0 - I_0\alpha(\nu)L \tag{B.5}$$

$$= I_0 - I_0\alpha(\bar{\nu} + a\cos(\omega t))L \tag{B.6}$$

The time dependent part is then expanded in a Taylor series about $\nu = \bar{\nu}$:

$$\alpha(\bar{\nu} + a\cos(\omega t)) = \alpha(\bar{\nu}) + \frac{d\alpha}{d\nu}\bigg|_{\nu=\bar{\nu}}(a\cos(\omega t)) + \frac{1}{2!}\frac{d^2\alpha}{d\nu^2}\bigg|_{\nu=\bar{\nu}}(a\cos(\omega t))^2 \tag{B.7}$$

$$+\frac{1}{3!}\frac{d^3\alpha}{d\nu^3}\bigg|_{\nu=\bar{\nu}}(a\cos(\omega t))^3 + \frac{1}{4!}\frac{d^4\alpha}{d\nu^4}\bigg|_{\nu=\bar{\nu}}(a\cos(\omega t))^4 + \cdots$$

Using identities for the powers of cosine gives:

$$\alpha(\bar{\nu} + a\cos(\omega t)) = \alpha(\bar{\nu}) + \frac{d\alpha}{d\nu}\bigg|_{\nu=\bar{\nu}}(a\cos(\omega t)) + \frac{a^2}{2!}\frac{d^2\alpha}{d\nu^2}\bigg|_{\nu=\bar{\nu}}\left(\frac{1}{2} + \frac{1}{2}\cos(2\omega t)\right) \tag{B.8}$$

$$+\frac{a^3}{3!}\frac{d^3\alpha}{d\nu^3}\bigg|_{\nu=\bar{\nu}}\left(\frac{1}{4}\right)(3\cos(\omega t) + \cos(3\omega t))$$

$$+\frac{a^4}{4!}\frac{d^4\alpha}{d\nu^4}\bigg|_{\nu=\bar{\nu}}\left(\frac{1}{8}\right)(3 + 4\cos(2\omega t) + \cos(4\omega t)) + \cdots$$

Collecting terms with the same frequency gives:

$$\alpha(\bar{\nu} + a\cos(\omega t)) = \alpha(\bar{\nu}) + \left(\frac{1}{2}\frac{1}{2!}\frac{d^2\alpha}{d\nu^2}\bigg|_{\nu=\bar{\nu}} a^2 + \frac{3}{8}\frac{1}{2!}\frac{d^4\alpha}{d\nu^4}\bigg|_{\nu=\bar{\nu}} a^4 + \cdots \right)$$

$$+ \left(\frac{d\alpha}{d\nu}\bigg|_{\nu=\bar{\nu}} a + \frac{3}{4}\frac{1}{3!}\frac{d^3\alpha}{d\nu^3}\bigg|_{\nu=\bar{\nu}} a^3 + \cdots \right)\cos(\omega t)$$

$$+ \left(\frac{1}{2}\frac{1}{2!}\frac{d^2\alpha}{d\nu^2}\bigg|_{\nu=\bar{\nu}} a^2 + \frac{1}{2}\frac{1}{4!}\frac{d^4\alpha}{d\nu^4}\bigg|_{\nu=\bar{\nu}} a^4 + \cdots \right)\cos(2\omega t)$$

$$+ \left(\frac{1}{4}\frac{1}{3!}\frac{d^3\alpha}{d\nu^3}\bigg|_{\nu=\bar{\nu}} a^3 + \cdots \right)\cos(3\omega t)$$

$$+ \left(\frac{1}{8}\frac{1}{4!}\frac{d^3\alpha}{d\nu^3}\bigg|_{\nu=\bar{\nu}} a^4 + \cdots \right)\cos(4\omega t) + \cdots \tag{B.9}$$

Reid and Labrie write the equation above in the following short-hand notation:

$$\alpha(\bar{\nu} + a\cos(\omega t)) = \sum_{n=0}^{\infty} H_n(\bar{\nu})\cos(n\omega t) \tag{B.10}$$

where

$$H_n(\bar{\nu}) = \frac{2^{1-n}}{n!}\alpha^n \frac{d^n\alpha(\nu)}{d\nu^n}\bigg|_{\nu=\bar{\nu}}, n \geq 1 \tag{B.11}$$

The sinusoidal modulation amplitude is 4 mV, which small relative to the mean scanning amplitude of 100 mV (smallest sinusoidal output from SR830 is 4 mV). For very small modulations such that $a \ll 1$:

$$\alpha(\bar{\nu} + a\cos(\omega t)) \approx \alpha(\bar{\nu}) + a\frac{d\alpha}{d\nu}\bigg|_{\nu=\bar{\nu}}\cos(\omega t) + \frac{a^2}{2}\frac{1}{2!}\frac{d^2\alpha}{d\nu^2}\bigg|_{\nu=\bar{\nu}}\cos(2\omega t)$$

$$+ \frac{a^3}{4}\frac{1}{3!}\frac{d^3\alpha}{d\nu^3}\bigg|_{\nu=\bar{\nu}}\cos(3\omega t) + \frac{a^4}{8}\frac{1}{4!}\frac{d^4\alpha}{d\nu^4}\bigg|_{\nu=\bar{\nu}}\cos(4\omega t) + \cdots \tag{B.12}$$

A lock-in amplifier is used to selectively amplify the second harmonic term, which is proportional to

$$\frac{a^2}{2}\frac{1}{2!}\frac{d^2\alpha}{d\nu^2}\bigg|_{\nu=\bar{\nu}}\cos(2\omega t) \ . \tag{B.13}$$

Derivatives of $\alpha(\nu)$, assuming a Lorentzian line shape, are:

$$\alpha(\nu) = \frac{\alpha_0}{1 + \left[\frac{\nu - \nu_0}{\Delta\nu}\right]^2} = \frac{\alpha_0 \Delta\nu^2}{\Delta\nu^2 + (\nu - \nu_0)^2} \tag{B.14}$$

$$\frac{d\alpha(\nu)}{d\nu} = -\frac{2\alpha_0 \Delta\nu^2 (\nu - \nu_0)}{(\nu^2 - 2\nu\nu_0 + \nu_0^2 + \Delta\nu^2)^2} = -\frac{2\alpha_0 \Delta\nu^2 (\nu - \nu_0)}{((\nu - \nu_0)^2 + \Delta\nu^2)^2} \tag{B.15}$$

$$\frac{d^2\alpha(\nu)}{d\nu^2} = \frac{2\alpha_0 \Delta\nu^2 (3\nu^2 - 6\nu\nu_0 + 3\nu_0^2 - \Delta\nu^2)}{(\nu^2 - 2\nu\nu_0 + \nu_0^2 + \Delta\nu^2)^3} = \frac{2\alpha_0 \Delta\nu^2 (3(\nu - \nu_0)^2 - \Delta\nu^2)}{((\nu - \nu_0)^2 + \Delta\nu^2)^3} \tag{B.16}$$

Evaluating at $\nu = \nu_0 = \bar{\nu}$ gives:

$$\left.\frac{d^2\alpha(\nu)}{d\nu^2}\right|_{\nu=\nu_0=\bar{\nu}} = -\frac{2\alpha_0}{\Delta\nu^2} \tag{B.17}$$

$$\left.\frac{d^2 I}{d\nu^2}\right|_{\nu=\nu_0=\bar{\nu}} = \frac{2\alpha_0 I_0 L}{\Delta\nu^2} \exp\left(-\alpha_0 L\right) \tag{B.18}$$

Finally the absorption coefficient, α_0 also equal to the product of the absorption cross section, σ_ν, and the number of molecules in the volume, n, as done in the previous section, $\alpha(\nu) = \sigma_\nu n$, giving:

$$\left.\frac{d^2 I}{d\nu^2}\right|_{\nu=\nu_0=\bar{\nu}} = \frac{2 I_0 L \sigma_\nu}{\tilde{R} T \Delta\nu^2} P \exp\left(-\frac{\sigma_\nu L}{\tilde{R} T} P\right) \tag{B.19}$$

In the actual application, the exponential term can be expanded in a Taylor series. A constant should be added to account for the air outside the test section and the coefficients of the series are obtained by calibration.

$$\left.\frac{d^2 I}{d\nu^2}\right|_{\nu=\nu_0=\bar{\nu}} = c_0 + c_1 P + c_2 P^2 + \cdots \tag{B.20}$$

The constants, c_0, c_1, and c_2, must be calibrated before the experiment and for relatively small amounts of oxygen a linear fit is sufficient.

B.1 Experimental Setup Addendum

The following section gives additional information to the experimental setup for oxygen detector not covered in section 2.2.3.1.

The laser diode used is a ULM763-03-TN-S46FTT, manufactured by Laser Components. The laser is tunable from 760 nm to 766 nm via current and temperature control. This allows for scanning across the absorption line. In our experiments the current is modulated, using a Thorlabs LDC 200 C

producing 20 mA, and temperature held constant by a Thorlabs TED 2002 C temperature controller. The detectors used are large-area, visible-spectrum-amplified Si detectors, Thorlabs PDA100A. The modulation signal is generated by adding the sine wave generated by the lock-in amplifier, Stanford Research System SR830, with a sawtooth wave generated by a function generator, Stanford Research Systems DS345, in a summing amplifier, Stanford Research System SIM980 powered independently without a SIM900 mainframe. The final signal can be amplified and bandpass filtered using a preamplifier like a Stanford Research Systems SR560.

The sweeping frequency can be adjusted from the 80 Hz mentioned to suit the needs of the experiment (Rieker et al., 2009), but was not changed significantly during this study. For the current configuration of 80 Hz sweep and 23.5 kHz modulation frequency a time constant of 100 μs is found to give good 1f (fundamental harmonic) and 2f (2nd harmonic) signals without excessive noise. The modulation depth of 4 mA can also be changed to maximize the 2f signal (Rieker, 2009). The signal can be amplified and bandpass filtered either before the lock-in amplifier and afterwards. An example of the signal is shown in Figure B.1 including the gate signal extracted from the synchronization signal produced by the signal generator that creates the sawtooth wave.
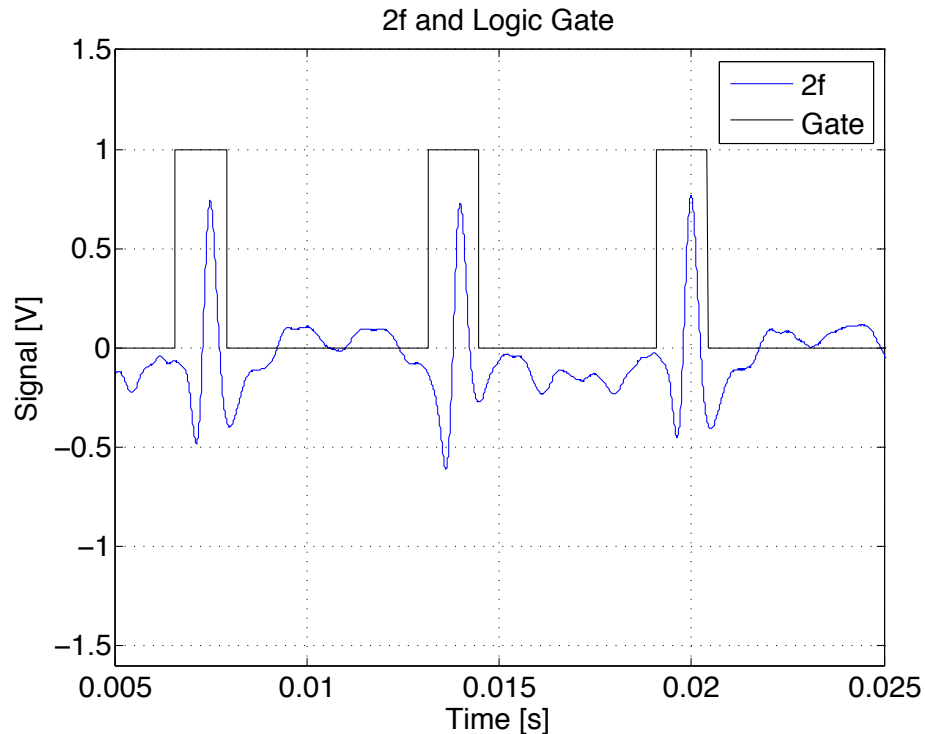

Figure B.1: Raw oxygen 2f data from shot 19

The measurements drifted significantly during the test time due to temperature changes of the

vessel and subsequent beam-steering and internal reflections in the windows (etalon). Some of the drifting can be accounted for by normalizing the 2f signal by the 1f intensity at the time of the 2f peak height (see Rieker et al. (2009)). However, for the large temperature changes imposed during the auto-ignition tests, the effects were generally too large to be compensated for using this method. The only reasonable data set is shown Figure 2.8 in section 2.2.3.2. The data was obtained by normalizing the drift using data obtained during the next experiment where the fuel was replaced by additional nitrogen in the mixture and all other parameters were kept the same.

For experiments with large temperature changes in the optical equipment, such as the windows, the 2f technique is not recommended.

Appendix C

Heated Vessel Theory

C.1 Governing Equation and Nomenclature

Recall Equation 2.5 from the discussion using the detailed chemical mechanism

$$V \rho c_v \frac{dT}{dt} = V \sum_{i=1}^{k} \dot{\omega}_i u_i + Sh \left(T_w^0 + \alpha\, t - T \right) = \dot{q}_r + \dot{q}_w. \tag{C.1}$$

with the following nomenclature.

Table C.1: Nomenclature

Parameter	Units	Description
T	K	gas temperature
V	m^3	volume
ρ	$kg\ m^{-3}$	density
c_v	$J\ kg^{-1}\ K^{-1}$	specific heat at constant
q_c	$J\ kg^{-1}$	chemical heat release (heat of combustion)
$\dot{\omega}_i$	$kg\ m^{-3}\ sec^{-1}$	net production rate per unit volume
u_i	$J\ kg^{-1}$	internal energy
S	m^2	surface area
h	$J\ sec^{-1}\ m^{-2}\ K^{-1}$	heat transfer coefficient
T_w^0	K	initial wall temperature
α	$K\ sec^{-1}$	wall temperature heating rate
$\dot{q}_r$	$J\ sec^{-1}$	energy release rate
$\dot{q}_l$	$J\ sec^{-1}$	energy loss rate

We now simplify the model such that we use a first order one-step Arrhenius rate for the consumption of the fuel, the governing equations for the reactor are:

$$V\rho c_v \frac{dT}{dt} = VQ\frac{d\lambda}{dt} - Sh\left(T - T_w\right) \tag{C.2}$$

$$\frac{d\lambda}{dt} = A\left(1 - \lambda\right)\exp\left(-\frac{E_a}{\tilde{R}T}\right) \ . \tag{C.3}$$

The stored chemical energy per unit mass, q_c, is related to the energy density, Q, through the density, ρ, by

$$Q = \rho q_c \ . \tag{C.4}$$

Table C.2: Additional nomenclature

Parameter	Units	Description
T_w	K	wall temperature
Q	$\mathrm{J\ m^{-3}}$	energy density
λ		progress variable
A	$\mathrm{sec^{-1}}$	pre-exponential
E_a	$\mathrm{J\ kmol^{-1}}$	activation energy
$\tilde{R}$	$\mathrm{J\ kmol^{-1}\ K^{-1}}$	universal gas constant

C.2   Induction Time

If we take the energy equation for a spatially homogeneous reactive material and assume a first order one-step Arrhenius rate,

$$\rho c_v \frac{dT}{dt} = QA\left(1 - \lambda\right)\exp\left(-\frac{E_a}{\tilde{R}T}\right) - \frac{Sh}{V}\left(T - T_w\right) \tag{C.5}$$

$$\frac{d\lambda}{dt} = A\left(1 - \lambda\right)\exp\left(-\frac{E_a}{\tilde{R}T}\right) \tag{C.6}$$

and now neglect fuel consumption and heat loss.

$$\frac{dT}{dt} = \frac{QA}{\rho c_v}\exp\left(-\frac{E_a}{\tilde{R}T}\right) \tag{C.7}$$

let $k = (QA)/(\rho c_v)$ and $\zeta = (E_a)/(\tilde{R}T)$ and integrate the equation to find the finite time at which the temperature tends to infinity.

$$\frac{d\zeta}{dT} = -\left(\frac{E_a}{\tilde{R}T}\right)^{-1} = -\frac{\tilde{R}}{E_a}\zeta^2 \implies dT = -\frac{E_a}{\tilde{R}}\frac{d\zeta}{\zeta^2}$$

$$k\int_0^t dt' = -\frac{E_a}{\tilde{R}}\int_{\zeta_0}^{\zeta}\frac{\exp\left(\zeta\right)}{\zeta^2}d\zeta$$

$$kt = \frac{E_a}{\tilde{R}}\int_{\zeta}^{\zeta_0}\frac{\exp\left(\zeta\right)}{\zeta^2}d\zeta \tag{C.8}$$

Using integration by parts we can proceed until further approximations must be made. $\int u\,dv = uv| - \int v\,du$ with $v = \exp\left(\zeta\right)$ and $u = \zeta^{-n}$

$$\int_{\zeta}^{\zeta_0}\frac{\exp\left(\zeta\right)}{\zeta^2}d\zeta = \frac{\exp\left(\zeta\right)}{\zeta^2}\bigg|_{\zeta}^{\zeta_0} + \int_{\zeta}^{\zeta_0}2\frac{\exp\left(\zeta\right)}{\zeta^3}d\zeta$$

$$\int_{\zeta}^{\zeta_0}\frac{\exp\left(\zeta\right)}{\zeta^2}d\zeta = \frac{\exp\left(\zeta\right)}{\zeta^2}\bigg|_{\zeta}^{\zeta_0} + 2\left[\frac{\exp\left(\zeta\right)}{\zeta^3}\bigg|_{\zeta}^{\zeta_0} + \int_{\zeta}^{\zeta_0}3\frac{\exp\left(\zeta\right)}{\zeta^4}d\zeta\right]$$

$$\int_{\zeta}^{\zeta_0}\frac{\exp\left(\zeta\right)}{\zeta^2}d\zeta = \left[\frac{\exp\left(\zeta\right)}{\zeta^2}\left(1 + \frac{2}{\zeta} + \cdots + \frac{(n+1)!}{\zeta^n} + \cdots\right)\right]_{\zeta}^{\zeta_0}$$

To leading order

$$t = \frac{E_a}{k\tilde{R}}\left(\frac{\exp\left(\zeta_0\right)}{\zeta_0{}^2} - \frac{\exp\left(\zeta\right)}{\zeta^2}\right) \tag{C.9}$$

Note: $T \to \infty$ (i.e., $\zeta \to 0$) as $t \to \infty$ because fuel consumption has been neglected. From equation C.7 we see that $dT/dt \to (QA)/(\rho c_v)$ as $T \to \infty$. We must thus chose a criterion for the temperature, which classifies ignition. Numerical integration of C.7 shows an inflection point in the temperature, which may be a suitable reference point.

$$\frac{dT}{dt} = \frac{QA}{\rho c_v} \exp\left(-\frac{T_a}{T}\right)$$

$$\frac{d^2T}{dt^2} = \left(\frac{QA}{\rho c_v}\right)^2 \frac{T_a}{T^2} \exp\left(-2\frac{T_a}{T}\right)$$

$$\frac{d^3T}{dt^3} = 2\left(\frac{QA}{\rho c_v}\right)^3 \frac{T_a(Ta-T)}{T^4} \exp\left(-3\frac{T_a}{T}\right)$$

$$\frac{d^3T}{dt^3} = 0 \to T = T_a$$

At the inflection point, the temperature has reached the activation temperature, which is corollary to rapid chemical reaction. $T = T_a$ implies $\zeta = 1$, which now allows us to evaluate C.9

$$t = \frac{E_a}{k\tilde{R}}\left(\frac{\exp(\zeta_0)}{\zeta_0{}^2} - e\right)$$

Recall that $\zeta_0 = T_a/T_0$

$$t = \frac{E_a}{k\tilde{R}}\left(\frac{\exp(T_a/T_0)}{(T_a/T_0)^2} - e\right)$$

Thus for large activation energy (i.e., large activation temperature), the first term completely dominates and we conclude that the induction time, τ_c, is

$$\tau_c = \frac{\rho c_v}{QA} \frac{\tilde{R}T_0{}^2}{E_a} \exp\left(\frac{E_a}{\tilde{R}T_0}\right) \tag{C.10}$$

C.2.1 Alternative Derivation

We can find the same induction time via a slightly different route. Starting from the heat equation without losses or consumption

$$\frac{dT}{dt} = \frac{QA}{\rho c_v} \exp\left(-\frac{E_a}{\tilde{R}T}\right) \ , \tag{C.11}$$

let $\phi = \tilde{R}T/E_a$, $k = QA/\rho c_v$

$$\frac{d\phi}{dt} = \frac{k\tilde{R}}{E_a} \exp\left(-\frac{1}{\phi'}\right) \tag{C.12}$$

$$\frac{k\tilde{R}}{E_a}\int_0^t dt' = \int_{\phi_0}^\phi \exp\left(\frac{1}{\phi'}\right) d\phi' \tag{C.13}$$

where $\phi_0 = \tilde{R}T_0/E_a$, and $\phi_{max} = \tilde{R}T_{max}/E_a$, where T_{max} is the maximum temperature reached if fuel consumption was included. The temperatures scale as follows

$$1 < \exp\left(\frac{1}{\phi_{max}}\right) < \exp\left(\frac{1}{\phi}\right) < \exp\left(\frac{1}{\phi_0}\right)$$

as $\phi_0 \ll 1 \implies e^{\frac{1}{\phi_0}} \gg 1$.

The limit of the integrand as T or ϕ tend to ∞ is 1 and thus the integral diverges as $\phi \to \infty$. Let us separate the integral into 2 components.

$$t\frac{k\tilde{R}}{E_a} = \int_{\phi_0}^\phi \exp\left(\frac{1}{\phi'}\right) d\phi' = \int_{\phi_0}^\phi \left(\exp\left(\frac{1}{\phi'}\right) - 1\right) d\phi' + \int_{\phi_0}^\phi d\phi' = I + II$$

However, within finite time, i.e., as ϕ approaches ϕ_{max}, I dominates the integral, so the induction time can be approximated as follows.

$$\tau_c = \frac{E_a}{k\tilde{R}}\int_{\phi_0}^{\phi_{max}} \left(\exp\left(\frac{1}{\phi'}\right) - 1\right) d\phi' \tag{C.14}$$

Make a change of variables as follows.

$$x = \frac{\phi_0}{\phi'} \;\; ; \;\; d\phi' = -\frac{\phi_0}{x^2}dx \;\; ; \;\; \exp\left(\frac{1}{\phi'}\right) = \exp\left(\frac{x}{\phi_0}\right)$$

$$\tau_c = \frac{E_a}{k\tilde{R}}\phi_0 \int_\epsilon^1 \frac{\left(\exp\left(\frac{x}{\phi_0}\right) - 1\right)}{x^2}dx \tag{C.15}$$

This integral is dominated by the contribution at $x = 1$ and thus we can integrate the equation and set $x = 1$.

$$\tau_c = \frac{E_a}{k\tilde{R}}\phi_0{}^2 e^{1/\phi_0} \tag{C.16}$$

Substituting back ϕ_0 and k gives

$$\tau_c = \frac{\rho c_v}{QA}\frac{T_0^2\tilde{R}}{E_a}\exp\left(\frac{E_a}{\tilde{R}T_0}\right). \tag{C.17}$$

C.2.2 Frank-Kamenetskii Approximation

We can follow the linearization by Frank-Kamenetskii (1969) about the initial temperature T_0, i.e., $T = T_0 + T'$. Using the geometric series

$$\frac{E_a}{\tilde{R}T} = \frac{E_a}{\tilde{R}(T_0 + T')} = \frac{E_a}{\tilde{R}T_0(1 + T'/T_0)} = \frac{E_a}{\tilde{R}T_0} - \frac{E_a}{\tilde{R}T_0^2}T' + \frac{E_a}{\tilde{R}T_0^3}T'^2 - \ldots \tag{C.18}$$

and neglecting higher order terms gives us

$$\frac{dT}{dt} = \frac{QA}{\rho c_v}\exp\left(-\frac{E_a}{\tilde{R}T_0}\right)\exp\left(\frac{E a T'}{\tilde{R}T_0^2}\right) \tag{C.19}$$

which we can now nondimensionalize the temperature as $\theta = (E_a T')/(\tilde{R}T_0^2)$, which will reveal the correct scaling for the time

$$\frac{d\theta}{dt} = \frac{QA}{\rho c_v}\frac{E_a}{\tilde{R}T_0^2}\exp\left(-\frac{E_a}{\tilde{R}T_0}\right)\exp\left(\theta\right)$$

$$\tau = t\frac{QA}{\rho c_v}\frac{E_a}{\tilde{R}T_0^2}\exp\left(-\frac{E_a}{\tilde{R}T_0}\right)$$

$$\frac{d\theta}{d\tau} = e^{\theta} \tag{C.20}$$

$$\int_0^{\tau} d\tau = \int_0^{\theta} e^{-\theta}d\theta$$

$$\theta = -\ln\left(1 - \tau\right) \tag{C.21}$$

We can now see see that the temperature will tend to $+\infty$ when $\tau = 1$, which is the induction time (τ_c).

$$\tau_c = \frac{\rho c_v}{QA}\frac{\tilde{R}T_0^2}{E_a}\exp\left(\frac{E_a}{\tilde{R}T_0}\right) \tag{C.22}$$

C.2.3 Wall Temperature Ramp Without Chemistry

In future section we would like to treat the chemical reaction as a deviation from the underlying behavior induced by the wall temperature ramp. While the final result is obvious, the details are still of interest. Neglecting the chemical reaction gives the following equation:

$$\frac{dT}{dt} = \frac{Sh}{\rho V c_v} \left(T_w^0 + \alpha t - T\right) \; . \tag{C.23}$$

Once cast in the following form the equation can be integrated using the integrating factor,

$$\frac{dT}{dt} + \frac{T}{t_w} = \frac{T_w^0 + \alpha t}{t_w} \; , \tag{C.24}$$

such that the final solution is found to be

$$T(t) = T_w^0 + \alpha t + \alpha t_w \left(e^{-t/t_w} - 1\right) \; , \tag{C.25}$$

where $t_w = (\rho V c_v)/(Sh)$ is the wall heat transfer time. At early time, we can expand the exponential term.

$$T(t) = T_w^0 + \alpha t + \alpha t_w \left(1 - \frac{t}{t_w} + \frac{1}{2}\left(\frac{t}{t_w}\right)^2 - \cdots - 1\right) \tag{C.26}$$

$$= T_w^0 + \alpha t - \alpha t_w \frac{t}{t_w} + \frac{1}{2}\left(\frac{t}{t_w}\right)^2 - \cdots \tag{C.27}$$

$$= T_w^0 + \frac{1}{2}\left(\frac{t}{t_w}\right)^2 - \cdots \tag{C.28}$$

At later times, as $t/t_w \to \infty$

$$T(t) = T_w^0 + \alpha \left(t - t_w\right) \; , \tag{C.29}$$

which implies that the temperature follows the outside ramping with a lag.

C.2.4 Ramp Rate Reduced Induction Time

The induction can be reduced when the vessel is heated from the outside. This introduces the heating rate in the energy equation in the following form,

$$\frac{dT}{dt} = \frac{QA}{\rho c_v} \exp\left(-\frac{E_a}{\tilde{R}T}\right) + \alpha \; . \tag{C.30}$$

The chemical energy release is a perturbation above the rate at which the temperature is increased externally.

Following the high activation energy arguments we can write equation as follows:

$$\frac{d\theta}{dt} = \frac{QA}{\rho c_v} \frac{E_a}{\tilde{R}T_0^2} \exp\left(-\frac{E_a}{\tilde{R}T_0}\right) \exp\left(\theta\right) + \frac{\alpha E_a}{\tilde{R}T_0^2} \tag{C.31}$$

where

$$\theta = \frac{E_a T'}{\tilde{R}T_0^2} \ . \tag{C.32}$$

Now we can substitute

$$\tau = t \frac{QA}{\rho c_v} \frac{E_a}{\tilde{R}T_0^2} \exp\left(-\frac{E_a}{\tilde{R}T_0}\right) = \frac{t}{\tau_c} \tag{C.33}$$

$$a = \frac{\alpha E_a}{\tilde{R}T_0^2} \tag{C.34}$$

which gives

$$\frac{d\theta}{dt} = \exp\left(\theta\right) + \frac{a}{\tau_c} \ , \tag{C.35}$$

that can be integrated

$$\int_0^{\tau_{ign}} d\tau = \int_0^{\theta_a} \frac{1}{e^\theta + \frac{a}{\tau_c}} d\theta = \int_0^{\theta_a} \frac{1}{e^\theta + \beta} d\theta \ , \tag{C.36}$$

where $\beta = a/\tau_c$.

$$\tau = \left[\frac{\theta - \ln\left(\beta + e^\theta\right)}{\beta}\right]_0^\theta \tag{C.37}$$

$$\tau = \frac{1}{\beta}\left(\theta - \ln\left(\frac{\beta + e^\theta}{\beta + 1}\right)\right) \tag{C.38}$$

$$\tau = \tau_c \frac{\tilde{R}T_0^2}{\alpha E_a}\left(\theta - \ln\left(\frac{\beta + e^\theta}{\beta + 1}\right)\right) \tag{C.39}$$

$$\tau = \tau_c \frac{\tilde{R}T_0^2}{\alpha E_a}\left(\frac{E_a T'}{\tilde{R}T_0^2} - \ln\left(\frac{\beta + e^\theta}{\beta + 1}\right)\right) \tag{C.40}$$

$$\tau = \frac{\tau_c}{\alpha}\left(T' - \frac{\tilde{R}T_0^2}{E_a} \ln\left(\frac{\beta + e^\theta}{\beta + 1}\right)\right) \tag{C.41}$$

C.2.5 Critical Heat-Loss Rate With Constant Wall Temperature

If we take the energy equation with heat loss to the wall, but keep the wall temperature constant and omit fuel consumption we arrive the classical Semenov model (Semenov, 1940). Following Law (2006, Combustion Physics, chapter 8.1.3), we can obtain the critical heat transfer coefficient.

$$\rho c_v \frac{dT}{dt} = QA \exp\left(-\frac{E_a}{\tilde{R}T}\right) - \frac{Sh}{V}(T - T_w) \tag{C.42}$$

T_w is the wall temperature to which the heat is lost, which may or may not be equal to the initial temperature T_0. Following the earlier perturbation and nondimensionalization we get

$$\frac{d\theta}{d\tau} = e^\theta - \hat{h}\left(\theta + \frac{T_a}{T_0}(T_0 - T_w)\right) \tag{C.43}$$

where $\hat{h} = \tau_c/\tau_l$ with $\tau_l = \rho V c_v/Sh$, which is the characteristic heat-loss time, and as before $\tau_c = \rho c_v \tilde{R}T_0{}^2/QAE_a \exp\left(E_a/\tilde{R}T_0\right)$.

For the case where $T_0 = T_w$, there exist solutions for $d\theta/d\tau = 0$ as long as $\hat{h} > e$. $\hat{h} = e$ is the critical heating transfer coefficient with values below e always leading to explosion, while for values of $\hat{h}$ higher than e the initial temperature ultimately determines the stability.

$$\frac{d\theta}{d\tau} = e^\theta - \hat{h}\theta \tag{C.44}$$

$$\frac{d\theta}{d\tau} = 0 \implies e^\theta = \hat{h}\theta \tag{C.45}$$

$$\frac{d}{d\theta} \implies e^\theta = \hat{h} \tag{C.46}$$

critical conditions for $\theta = 1$ and $\hat{h} = e$.

C.3 Full Nondimensional Equations

$$\rho c_v \frac{dT}{dt} = QA(1-\lambda)\exp\left(-\frac{E_a}{\tilde{R}T}\right) + \frac{Sh}{V}(T_w + \alpha t - T) \tag{C.47}$$

$$\frac{d\lambda}{dt} = A(1-\lambda)\exp\left(-\frac{E_a}{\tilde{R}T}\right) \tag{C.48}$$

Here we make no assumptions about the activation energy or fuel consumption. Let $T_a = E_a/\tilde{R}$.

$$\frac{dT}{dt} = (1-\lambda)\frac{1}{\tau_c}\exp\left(\frac{T_a}{T_0} - \frac{T_a}{T}\right) + \frac{1}{\tau_l}(T_w + \alpha t - T) \tag{C.49}$$

$$\frac{d\left(TT_a/T_0{}^2\right)}{d\left(t/\tau_c\right)} = (1-\lambda)\exp\left(\frac{T_a}{T_0} - \frac{T_a}{T_0{}^2}\left(\frac{T_0{}^2}{TT_a}\right)\right) - \frac{\tau_c}{\tau_l}\left(\frac{T_w T_a}{T_0{}^2} + \alpha t - \left(\frac{TT_a}{T_0{}^2}\right)\right) \tag{C.50}$$

let $\theta = TT_a/T_0^2$, $\theta_0 = T_a/T_0$, $\theta_w = T_w T_a/T_0{}^2$, $\tau = t/\tau_c$, $\hat{h} = \tau_c/\tau_l$, $\tilde{\alpha} = \alpha\tau_c T_a/T_0{}^2$, $A^* = A\tau_c$

$$\frac{d\theta}{d\tau} = (1-\lambda)\exp\left(\theta_0 - \frac{\theta_0{}^2}{\theta}\right) + \hat{h}\left(\theta_w + \tilde{\alpha}\tau - \theta\right) \tag{C.51}$$

$$\frac{d\lambda}{d\tau} = A^*(1-\lambda)\exp\left(-\frac{\theta_0{}^2}{\theta}\right) \tag{C.52}$$

If we assume that the initial wall temperature is equal to the initial gas temperature, then $\theta_w = \theta_0$, thus slightly simplifying C.51 to:

$$\frac{d\theta}{d\tau} = (1-\lambda)\exp\left(\theta_0 - \frac{\theta_0{}^2}{\theta}\right) + \hat{h}\left(\theta_0 + \tilde{\alpha}\tau - \theta\right) \tag{C.53}$$

Appendix D

Collision Limit Calculation for Pre-Exponential

For bimolecular reactions,

$$R_1 + R_2 \rightarrow P_1 + P_2 \tag{D.1}$$

the reaction rate is limited by the collision limit, i.e., R_1 and R_2 cannot react faster that the rate at which they collide. The collision rate between two dislike molecules per unit volume and time is given in Vincenti and Kruger (1967) as

$$Z_{R_1 R_2} = n_{R_1} n_{R_2} d_{R_1 R_2}^2 \left(\frac{8 \pi k T}{m_{R_1 R_2}^*} \right)^{1/2} . \tag{D.2}$$

The reaction rate of R_1 can thus be expressed as

$$-\frac{d\,[R_1]}{dt} = Z_{R_1 R_2} \frac{1}{N_{AV}} \exp \left(-\frac{E_a}{\tilde{R}T} \right) . \tag{D.3}$$

Assuming that the mixture is slightly off stoichiometric gives

$$[R_1] = [R_1]_0 \, (1 - \lambda) \tag{D.4}$$

$$[R_2] \approx [R_2]_0 . \tag{D.5}$$

Substituting back into the equation gives

$$\frac{d\lambda}{dt} \, [R_1]_0 = n_{R_1} n_{R_2} d_{R_1 R_2}^2 \left(\frac{8 \pi k T}{m_{R_1 R_2}^*} \right)^{1/2} \frac{1}{N_{AV}} \exp \left(-\frac{E_a}{\tilde{R}T} \right) . \tag{D.6}$$

Noting that $n_{R_1} = [R_1] N_{AV} = [R_1]_0 (1 - \lambda) N_{AV}$ and $n_{R_2} = [R_2] N_{AV} \approx [R_2]_0 N_{AV}$ gives

$$\frac{d\lambda}{dt} [R_1]_0 = [R_1]_0 (1 - \lambda) N_{AV} [R_2]_0 N_{AV} d^2_{R_1 R_2} \left(\frac{8\pi kT}{m^*_{R_1 R_2}} \right)^{1/2} \frac{1}{N_{AV}} \exp\left(-\frac{E_a}{\tilde{R} T} \right) , \quad \text{(D.7)}$$

which can be simplified to

$$\frac{d\lambda}{dt} = (1 - \lambda) [R_2]_0 N_{AV} d^2_{R_1 R_2} \left(\frac{8\pi kT}{m^*_{R_1 R_2}} \right)^{1/2} \exp\left(-\frac{E_a}{\tilde{R} T} \right) . \quad \text{(D.8)}$$

The simplified one-step model has been cast in the following way

$$\frac{d\lambda}{dt} = A (1 - \lambda) \exp\left(-\frac{E_a}{\tilde{R} T} \right) . \quad \text{(D.9)}$$

Thus we can find the limit for A using

$$A = [R_2]_0 N_{AV} d^2_{R_1 R_2} \left(\frac{8\pi kT}{m^*_{R_1 R_2}} \right)^{1/2} . \quad \text{(D.10)}$$

As a upper limit we can assume that R_2 is the oxygen concentration, which is

$$[R_2]_0 = \frac{P}{\tilde{R} T} X_{O_2} = 1 \text{ atm} \times \frac{\text{K mol}}{8.205746 \times 10^{-5} \text{ atm m}^3} \times \frac{1}{300 \text{ K}} \times 0.20 = 8.13 \frac{\text{mol}}{\text{m}^3} . \quad \text{(D.11)}$$

The collision cross section is

$$d^2_{R_1 R_2} = \left(\frac{2.92 \times 10^{-10} \text{ m} + 5.87 \times 10^{-10} \text{ m}}{2} \right)^2 = 1.9 \times 10^{-19} \text{ m}^2 . \quad \text{(D.12)}$$

The reduced mass is

$$m^*_{R_1 R_2} = \frac{m_{R_1} \times m_{R_2}}{m_{R_1} + m_{R_2}} = \frac{32 \text{ amu} \times 86 \text{ amu}}{32 \text{ amu} + 86 \text{ amu}} \times \frac{1.66 \times 10^{-27} \text{ kg}}{\text{amu}} = 5.39 \times 10^{-22} \text{ kg} . \quad \text{(D.13)}$$

Then A is

$$A = [R_2]_0 N_{AV} d^2_{R_1 R_2} \left(\frac{8\pi kT}{m^*_{R_1 R_2}} \right)^{1/2} \quad \text{(D.14)}$$

$$A = 8.13 \frac{\text{mol}}{\text{m}^3} \times \frac{6.022 \times 10^{23}}{\text{mol}} \times 1.9 \times 10^{-19} \text{ m}^2 \left(\frac{8\pi \times 1.3806503 \times 10^{-23} \text{ kg m}^2 \times 300 \text{ K}}{5.39 \times 10^{-22} \text{ kg s}^2 \text{ K}} \right)^{1/2}$$

$$A = 1.29 \times 10^7 \text{sec}^{-1}$$

Appendix E

Correlation of Hot Surface Ignition Temperature with Surface Area

Kuchta et al. (1965) presented their results for hot surface ignition as a function of hot surface size and created empirical correlations for various fuels. The analysis follows the analytical work performed by Semenov (1940) for cases considering conductive heat transfer only. The temperature profile is governed by the energy equation

$$\rho c_p \frac{dT}{dt} = k \frac{d^2 T}{dx^2} + \dot{q}_r \ . \tag{E.1}$$

The heat generated by chemical reaction is given by

$$\dot{q}_r = QA \left(1 - \lambda\right) \exp\left(-\frac{E_a}{\tilde{R}T}\right) \tag{E.2}$$

and the spatial temperature distribution at steady state is given by

$$-\lambda \frac{d^2 T}{dx^2} = \dot{q}_r \ . \tag{E.3}$$

Using the linearization as discussed in C.2.2 and neglecting consumption ($\lambda \approx 0$), the steady state equation becomes

$$\lambda \frac{d^2 T}{dx^2} = QA \exp\left(-\frac{E_a}{\tilde{R}T_1}\right) \exp\left(-\frac{E_a \left(T_1 - T\right)}{\tilde{R}T_1{}^2}\right) \ , \tag{E.4}$$

where T_1 is the temperature of the hot surface. The steady state case allows us to find a critical condition for the ignition.

The condition leading to ignition is traced back to van't Hoff and described in 2 different ways.

First, the condition for ignition is given as a zero temperature gradient at the hot surface, r_s,

$$\left.\frac{dT}{dr}\right|_{r=r_s} = 0 \ . \tag{E.5}$$

Second, as given by Semenov (1940) the point

"at which the plate does not lose heat and all the heat cold plate will be generated by the reaction taking place in a relatively narrow zone, ζ, near the hot plate."

This can be expressed by considering that the gas temperature at the wall is slightly higher than the wall itself and the heat transfer into the wall is equal to the heat transfer out of the gas

$$-k \left.\frac{dT_{gas}}{dx}\right|_{x=0} = h \left(T_w - T_{gas}(x=0)\right) \tag{E.6}$$

where k is the conductivity of the gas and h is the conductivity of the wall.

The energy equation (E.4) can be integrated across the small boundary near the heated wall by first multiplying through by dT/dx and integrating with respect to x:

$$-\int_0^\zeta \frac{dT}{dx}\frac{d^2T}{dx^2}dx = \int_0^\zeta \frac{QA}{k}\exp\left(-\frac{E_a}{\tilde{R}T_1}\right)\exp\left(-\frac{E_a\left(T_1-T\right)}{\tilde{R}T_1^2}\right)\frac{dT}{dx}dx \ . \tag{E.7}$$

The left-hand side can be simplified and the right-hand side can be reduced to an integration with respect to temperature:

$$-\int_0^\zeta \frac{1}{2}\frac{d}{dx}\left(\frac{dT}{dx}\right)^2 dx = \int_{T_1}^{T_e} \frac{QA}{k}\exp\left(-\frac{E_a}{\tilde{R}T_1}\right)\exp\left(-\frac{E_a\left(T_1-T\right)}{\tilde{R}T_1^2}\right)dT \ . \tag{E.8}$$

$$\left.\left(\frac{dT}{dx}\right)^2\right|_{x=0} - \left.\left(\frac{dT}{dx}\right)^2\right|_{x=\zeta} = \frac{2QA\tilde{R}T_1^2}{kE_a}\exp\left(-\frac{E_a}{\tilde{R}T_1}\right)\left(1-\exp\left(-\frac{E_a\left(T_1-T\right)}{\tilde{R}T_1^2}\right)\right) \tag{E.9}$$

The gradient at $x = \zeta$ is zero and the first term dominates the right-hand side in the regime of interest (Semenov, 1940, Laurendeau, 1982)

$$\left.\left(\frac{dT}{dx}\right)\right|_{x=0} = \sqrt{\frac{2QA\tilde{R}T_1^2}{kE_a}\exp\left(-\frac{E_a}{\tilde{R}T_1}\right)} \ . \tag{E.10}$$

Semenov (1940) gives the example of the a flammable gas between two plate, one hot at an elevated temperature T_1, and one cold at T_0. Considering only conduction, the temperature gradient is equal

to the temperature difference divided by the distance between the plates, d.

$$\frac{dT}{dx} = \frac{T_1 - T_0}{d} \tag{E.11}$$

So the ignition temperature T_1 can be related to the distance between two plates or equivalently to the size of a heated vessel (Frank-Kamenetskii, 1969, Kuchta et al., 1965).

$$d = \sqrt{\frac{kE_a \left(T_1 - T_0\right)^2}{2QA\tilde{R}T_1^2}} \exp\left(\frac{E_a}{\tilde{R}T_1}\right) \tag{E.12}$$

For ignition from hot spheres and wires a similar argument can be made. Consider a small hot sphere of radius R_S, which is inside a large vessel of radius, R_V ($R_V \gg r$), filled with flammable gas.

> "By assuming that the zone within which the reaction occurs extends to a distance $[\xi]$ from the surface of the sphere very much less than the radius of the sphere the problem, to an accuracy sufficient for our purposes, is reduced to the parallel plate case just considered." (Semenov, 1940)

The heat flux due to the chemical energy generated in the reaction zone is given by

$$\tilde{Q}_{\text{chem}} = 4\pi \left(R_S + \xi\right) \sqrt{\frac{2QA\tilde{R}T_1^2}{kE_a} \exp\left(-\frac{E_a}{\tilde{R}T_1}\right)}. \tag{E.13}$$

Outside the reaction zone, ξ, the temperature distribution is the same as for a non-reacting mixture, and given as function of the radial distance, r,

$$T - T_0 = \frac{\left(T_1 - T_0\right)\left(R_S + \xi\right)}{r}. \tag{E.14}$$

The heat flux through a sphere of radius $R_S + \xi$ is

$$\tilde{Q}_{\text{loss}} = 4\pi k \left(T_1 - T_0\right)\left(R_S + \xi\right). \tag{E.15}$$

Equating the heat release and loss flux, the relationship for ignition temperature for heated spheres

is given by Semenov (1940) to be

$$R_S = \left(\frac{E_a k \left(T_1 - T_0\right)^2}{2R_V T_1^2 Q A \exp\left(-E_a/(\tilde{R}T_1)\right)} \right)^{1/2} .$$

(E.16)

Similarly, Semenov arrives at the following relationship for the ignition temperature as a function of radius for heated wires of radius R_W,

$$R_W \ln \frac{R_V}{R_W} = \left(\frac{E_a k \left(T_1 - T_0\right)^2}{2R_V T_1^2 Q A \exp\left(-E_a/(\tilde{R}T_1)\right)} \right)^{1/2} .$$

(E.17)

Kuchta et al. (1965) simplifies this relationship by assuming that the exponential term dominates and expands the left-hand side and keeping only the leading order term,

$$r \sim \exp\left(E_a/(2\tilde{R}T_1)\right) .$$

(E.18)

Taking the natural logarithm of both sides yields

$$\ln r \sim \frac{1}{T_1}$$

(E.19)

which Kuchta et al. (1965) used to fit part of their data.

It seems that Kuchta et al. (1965) extended this relationship from the radius of the wire to the surface area by assuming a constant length and thus giving a linear relationship between the surface area and radius.

$$A = 2\pi r L$$

(E.20)

The results obtained in the current study are compared to the data and fit in Section 3.4.5 (see Figure 3.26). The data presented in Section 3.4.5 is limited to the lowest temperature observed as the equivalence ratio is varied. The higher ignition temperature near lower and upper flammability limit are not shown. For completeness all ignition data collected at various pressure and equivalence ratios is given in Figure E.1. We can observe some overlap with the historical data, but while the fit shown captures the overall trend of increasing the hot surface temperature required for ignition as the size of the hot surface decreases, it is insufficient in capturing the lowest temperature observed in this study. We would like to stress that control over composition, pressure as well as careful characterization of the hot surface temperature and geometry are necessary to fully assess safety

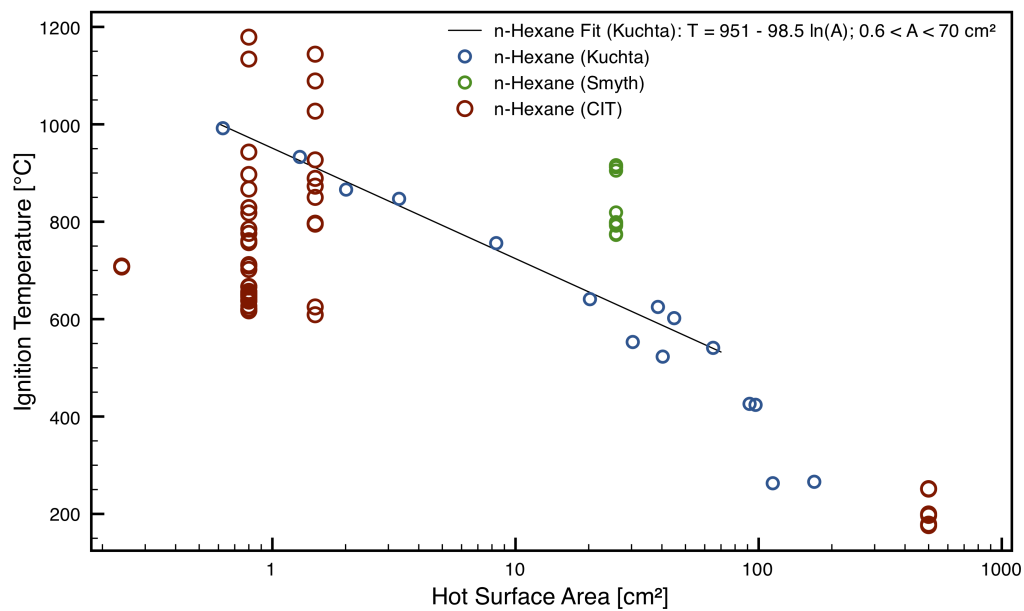hazards stemming from hot surfaces in contact with flammable mixtures.

Figure E.1: Ignition as a function of hot surface size (uncertainty in ignition temperature for CIT measurements is +110 K). Range in values for CIT measurements is due to a range of compositions and initial pressure.

This page intentionally left blank.
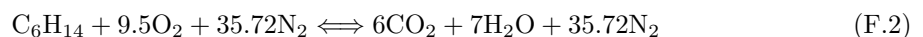
Appendix F

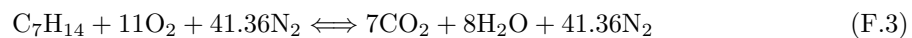# Flame Propagation

F.1   Introduction

A limited amount of data is available for the flame and burning speed of n-hexane-air mixtures. Davis and Law (1998b) used a counterflow twin flame burner to systematically eliminate the effects of flame stretch. Kelley et al. (2011) performed experiments in a double-chambered vessel, basically eliminating the pressure rise during the flame propagation, while using schlieren visualization of the flame propagation and nonlinear extrapolation to the laminar burning speed to account for the effects of flame stretch. The accuracy of the mixture composition is verified using a gas chromatograph and flame ionization detector (Kelley et al., 2011). The range of equivalence ratios that can be investigated using this technique is limited due to the onset of hydrodynamic instabilities and thus at atmospheric pressure no flame speed data is available for equivalence ratios larger than $\phi = 1.7$ (Kelley et al., 2011).

At the current stage, the CaltechMech (Blanquart, 2011) has validated flame speeds for n-heptane only. In the simulations performed using the FlameMaster software (Pitsch and Bollig, 1994) n-heptane is substituted for n-hexane, which creates a slightly different mixture composition for complete oxidation as shown in Equations F.2 and F.3 and thus the results are shown as a function of equivalence ratio ϕ, where

$$\phi = \frac{N_{\text{fuel}}/N_{\text{oxidizer}}}{(N_{\text{fuel}}/N_{\text{oxidizer}})_{\text{stoichiometric}}} \ . \tag{F.1}$$

The balanced chemical equation give the stoichiometric ratio for n-hexane and n-heptane oxidation in air.

$$\text{C}_6\text{H}_{14} + 9.5\text{O}_2 + 35.72\text{N}_2 \Longleftrightarrow 6\text{CO}_2 + 7\text{H}_2\text{O} + 35.72\text{N}_2 \tag{F.2}$$

$$C_7H_{14} + 11O_2 + 41.36N_2 \Longleftrightarrow 7CO_2 + 8H_2O + 41.36N_2 \qquad \text{(F.3)}$$

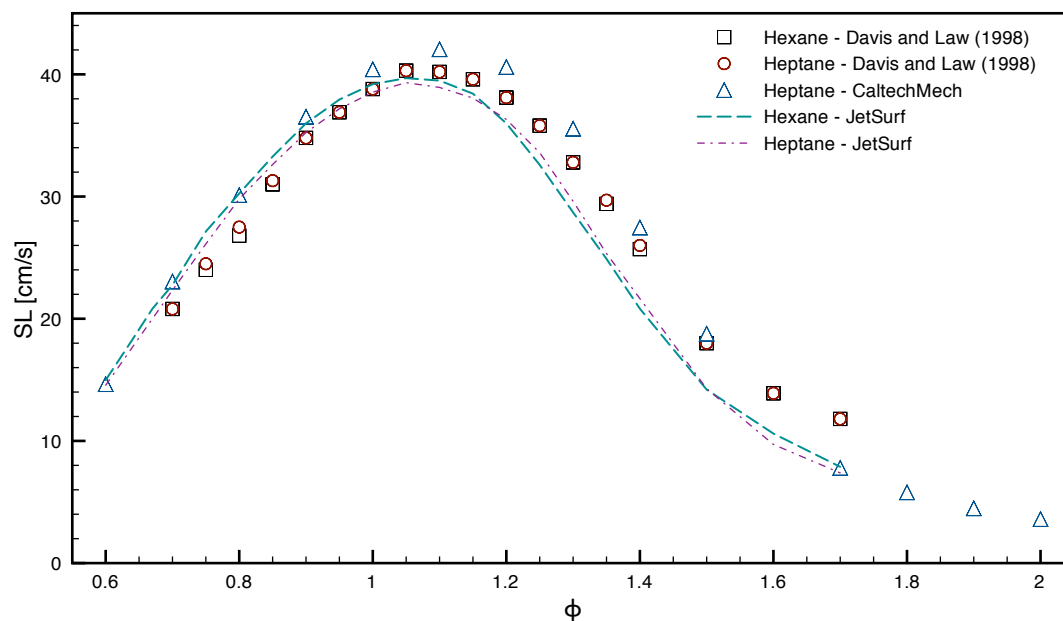## F.2 Flame Propagation Speed as a Function of Composition

Figure F.1: Laminar burning velocity at room temperature and atmospheric pressure for n-hexane and n-heptane (Davis and Law (1998b), JetSurF results from Wang et al. (2010))
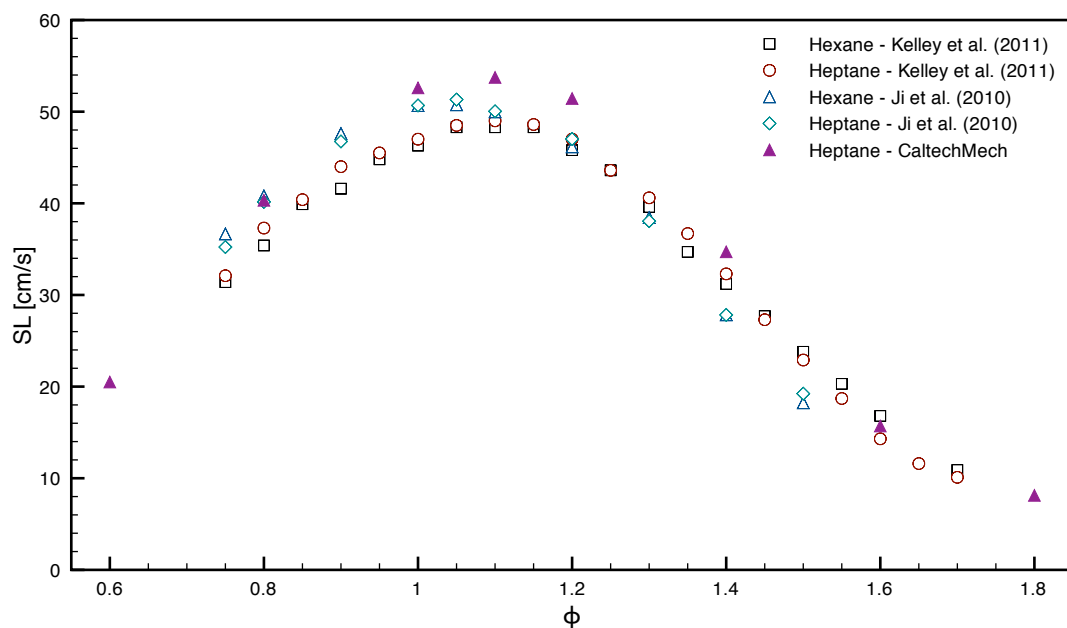
Figure F.2: Laminar burning velocity at 353 K and atmospheric pressure for n-hexane and n-heptane Kelley et al. (2011), Ji et al. (2010)
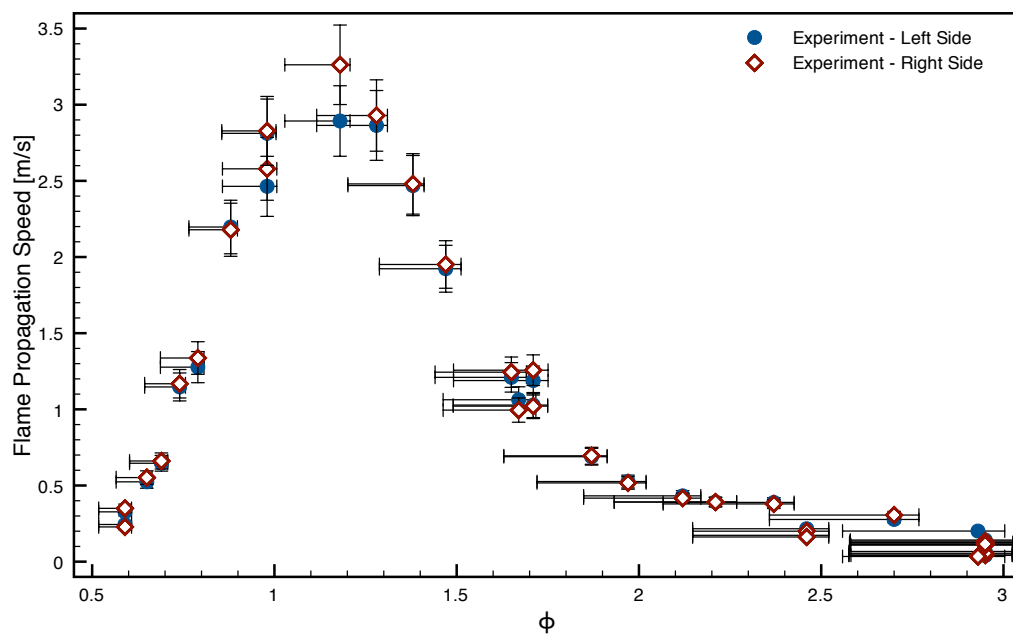

Figure F.3: Experimental flame propagation speed on the left and right side with measurement uncertainties. Initial pressure is one atmosphere with the mixture at room temperature (294 K).
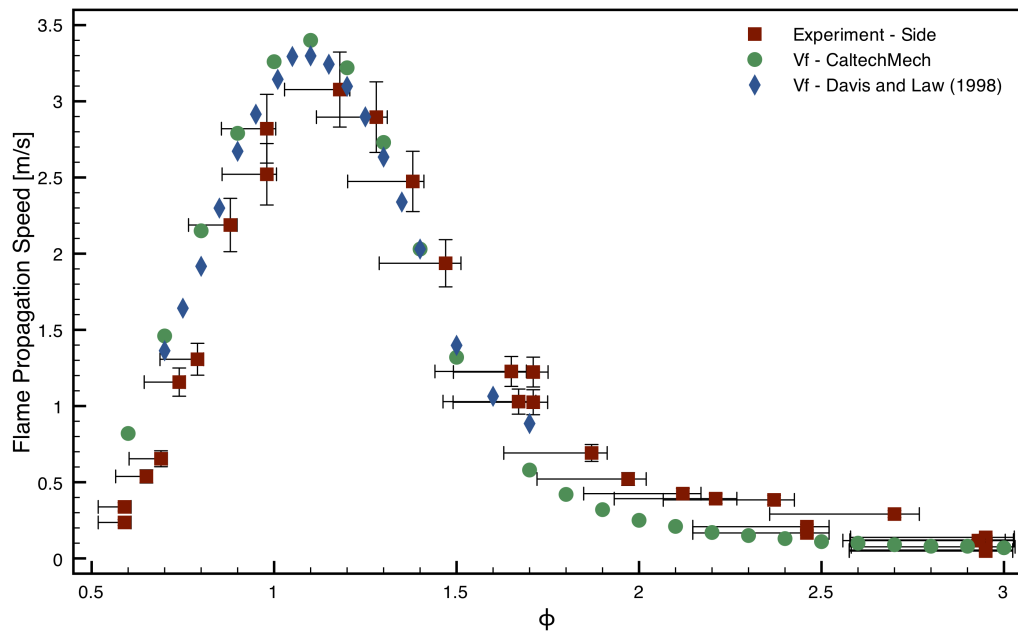
Figure F.4: Flame propagation speed at room temperature and atmospheric pressure including the estimated flame propagation speed from Davis and Law (1998b) calculated by multiplying the the laminar burning velocity by the expansion ratio obtained by equilibrating the mixture at constant pressure using the thermodynamic data from the Ramirez mechanism (Ramirez et al., 2011)

F.3 Tabular Flame Speed Data

Table F.1: Laminar burning velocity (s_L) for n-hexane and n-heptane at atmospheric pressure (P_0 = 101 kPa), room temperature (T_u = 300 K) digitized from Davis and Law (1998b) and at elevated temperature (T_u = 353 K) digitized from Kelley et al. (2011) and Ji et al. (2010)

	T_u = 300 K		T_u = 353 K		T_u = 353 K	
	Davis and Law (1998b)		Kelley et al. (2011)		Ji et al. (2010)	
	n-hexane	n-heptane	n-hexane	n-heptane	n-hexane	n-heptane
ϕ	S_l (cm/s)	S_l (cm/s)	S_l (cm/s)	S_l (cm/s)	S_l (cm/s)	S_l (cm/s)
0.75	23.98	24.52	31.44	32.14	36.66	35.23
0.80	26.82	27.54	35.40	37.25	40.81	40.16
0.85	30.96	31.30	39.85	40.43	-	-
0.90	34.79	34.79	41.58	43.95	47.61	46.75
0.95	36.89	36.89	44.80	45.45	-	-
1.00	38.82	38.82	46.29	46.95	50.66	50.68
1.05	40.28	40.28	48.27	48.54	50.75	51.32
1.10	40.18	40.18	48.27	48.99	49.98	50.04
1.15	39.62	39.62	48.27	48.55	-	-
1.20	38.05	38.05	45.79	46.97	46.16	47.02
1.25	35.84	35.84	43.56	43.63	-	-
1.30	32.80	32.80	39.60	40.55	38.44	38.06
1.35	29.35	29.66	34.65	36.69	-	-
1.40	25.67	25.98	31.19	32.29	27.83	27.82
1.45	-	-	27.72	27.28	-	-
1.50	17.97	17.97	23.76	22.88	18.23	19.23
1.55	-	-	20.30	18.75	-	-
1.60	13.91	13.91	16.83	14.26	-	-
1.65	-	-	-	11.62	-	-
1.70	11.78	11.78	10.89	10.13	-	-

F.4   Tabular Expansion Ratio Data

Table F.2: Expansion ratio for n-hexane and n-heptane at atmospheric pressure ($P_0 = 101$ kPa), room temperature ($T_u = 300$ K) computed using the thermodynamic data from the Ramirez mechanism (Ramirez et al., 2011)

ϕ	n-hexane ϵ	n-heptane ϵ	ϕ	n-hexane ϵ	n-heptane ϵ
0.55	5.53	5.55	1.80	7.38	7.46
0.60	5.88	5.90	1.85	7.31	7.39
0.65	6.21	6.24	1.90	7.24	7.32
0.70	6.54	6.57	1.95	7.17	7.25
0.75	6.85	6.88	2.00	7.09	7.18
0.80	7.15	7.18	2.05	7.02	7.11
0.85	7.43	7.46	2.10	6.94	7.03
0.90	7.68	7.72	2.15	6.87	6.96
0.95	7.90	7.94	2.20	6.79	6.88
1.01	8.10	8.14	2.25	6.71	6.81
1.05	8.18	8.22	2.30	6.63	6.73
1.10	8.21	8.25	2.35	6.55	6.65
1.15	8.19	8.23	2.40	6.47	6.57
1.20	8.14	8.19	2.45	6.39	6.49
1.25	8.09	8.14	2.50	6.31	6.41
1.30	8.03	8.09	2.55	6.22	6.33
1.35	7.97	8.03	2.60	6.14	6.24
1.40	7.91	7.97	2.65	6.05	6.16
1.45	7.85	7.91	2.70	5.96	6.07
1.50	7.78	7.85	2.75	5.88	5.99
1.55	7.72	7.79	2.80	5.79	5.90
1.60	7.65	7.72	2.85	5.70	5.81
1.65	7.58	7.66	2.90	5.62	5.73
1.70	7.52	7.59	2.95	5.55	5.66
1.75	7.45	7.52	3.00	5.49	5.60

Appendix G

Thermal Plume Scaling

We follow the arguments by Tritton (1988) to determine the thermal plume properties above the hot surface before ignition occurs. For steady flows without chemical reaction and with changes in density that are negligible except for when they create a buoyancy force (Boussinesq approximation), the following hold true for changes in density, continuity, momentum, and energy balance.

$$\Delta\rho = -\alpha\rho_0\Delta T \tag{G.1}$$

$$\frac{\partial u_i}{\partial x_i} = 0 \tag{G.2}$$

$$u_j\frac{\partial u_i}{\partial x_j} = -\frac{1}{\rho}\frac{\partial P}{\partial x_i} - \nu\frac{\partial^2 u_i}{\partial x_j^2} - g\hat{k}\alpha\Delta T \tag{G.3}$$

$$u_j\frac{\partial T}{\partial x_j} = \kappa\frac{\partial^2 T}{\partial x_j^2} \tag{G.4}$$

Neglecting pressure gradients, the inertial, viscous, and buoyancy terms are of the same magnitude in a laminar plume. In the vertical direction (z, $\hat{k}$), this gives the following scaling:

$$\frac{w_{max}^2}{z} \sim \frac{\nu w_{max}}{\delta^2} \sim g\alpha\Delta T \tag{G.5}$$

where w_{max} is the maximum vertical velocity in the plume, δ is the width of the plume, and z is the height above the plume. For a plume that is created from a small hot wire the maximum vertical velocity, w_{max}, and the maximum temperature difference, ΔT_{max}, occur along the centerline. From Equation G.5, the scaling of w_{max} and δ can be found as a function of the height above the source, z,

$$w_{max} \sim [g\alpha\Delta T z]^{1/2} \propto z^{1/2} \tag{G.6}$$

$$\delta \sim \left[\frac{\nu^2 z}{g\alpha\Delta T}\right]^{1/4} \propto z^{1/4} \tag{G.7}$$

The thermal plume behaves similarly to a jet, where vertical momentum is a conserved quantity at any cross section of the jet along its axis. For the thermal plume, the energy flux is conserved and the vertical momentum increases with distance due to buoyancy. Drawing a control volume around the source, $\dot{Q}$, and plume and applying energy conservation, we find that the quantity

$$\int_{CV} h\rho u_i n_i dA = \dot{Q} \tag{G.8}$$

is constant.

While we have a source of energy, there is not mass source and thus

$$\int_{CV} \rho u_i n_i dA = 0 \tag{G.9}$$

which by multiplying both sides by the the constant h_0, the enthalpy outside the plume gives

$$\int_{CV} h_0 \rho u_i n_i dA = 0. \tag{G.10}$$

Subtracting equation G.10 from G.8 and applying $h = c_p T$ gives

$$\int_{CV} c_p \left(T - T_0\right) \rho u_i n_i dA = \dot{Q} = const. \tag{G.11}$$

This equation must hold true for any control volume that includes the plume and source and thus

$$\frac{d}{dz} \int_{CV} c_p \left(T - T_0\right) \rho u_i n_i dA = 0 . \tag{G.12}$$

For the equation above to hold true, the integrand must be constant with respect to z, which implies

$$c_p \Delta T \rho w \delta \sim \text{constant} . \tag{G.13}$$

Using the scalings in Equation G.5

$$w \sim \frac{\nu z}{\delta^2} \tag{G.14}$$

$$\Delta T \sim \frac{\nu^2 z}{\delta^4 g\alpha} \tag{G.15}$$

gives

$$\frac{\nu^2 z}{\delta^4 g\alpha} \frac{\nu z}{\delta^2} \delta = \text{constant} , \tag{G.16}$$

which simplifies to

$$\frac{z^2}{\delta^5} = \text{constant} . \tag{G.17}$$

If we suppose a power scaling for the width, δ, with height, z,

$$\delta = z^m \tag{G.18}$$

then $m = 2/5$ such that the left-hand side of Equation G.17 is constant. This means that the maximum temperature difference (at the centerline) ΔT_{max}, the maximum velocity w_{max}, and the width δ scale as follows with the height above the source, z.

$$\Delta T_{max} \sim z^{-3/5}, w_{max} \sim z^{1/5}, \delta \sim z^{2/5} \tag{G.19}$$

With the temperature measurements taken using the thermocouple array, we can confirm the scaling of the temperature, ΔT, with height above the glow plug as shown Figure G.1. Due to the fact that the glow plug is an extended source, the scaling holds for the far field readings obtained further away from the glow plug.
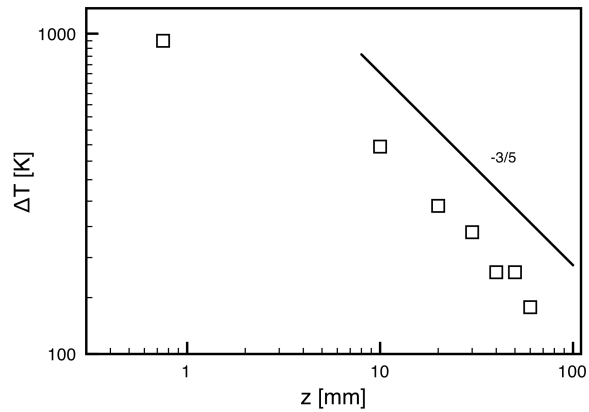

Figure G.1: Plume temperature scaling and thermocouple measurements taken using the thermocouple array.

This page intentionally left blank.

Appendix H

Refitting Thermodynamic Data [1]

Thermodynamic data, including specific heat, enthalpy and entropy for each species, are part of the chemical mechanism used to compute the ignition in the slowly heated vessel in Boettcher et al. (2011). In the thermodynamic data included as part of the mechanism published by Ramirez et al. (2011), many of the species have a discontinuity at the point where the low temperature fit connects to the high-temperature fit as shown in Figure H.1 for $C_2H_5CO_2$. These discontinuities are problematic for some numerical solvers and should be avoided.
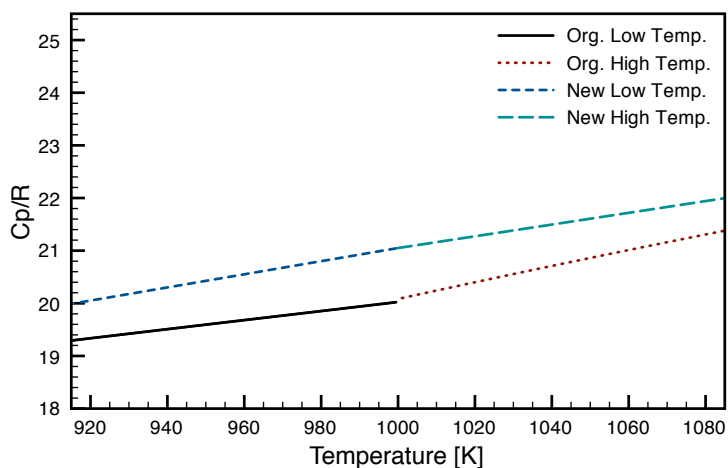

Figure H.1: Original thermodynamic data - c_p/R for $C_2H_5CO_2$

The NASA polynomial representation is used for complex equilibrium calculations as discussed by Gordon and McBride (1994). Further discussion of the polynomials and fitting is given in Shepherd et al. (2006)[2]. For each species the data has two sets of seven coefficients, a_n for the low temperature regime and seven coefficients, b_n for the high-temperature regime. For example, the

---

[1] The following work was based on a routine for fitting thermodynamic data created by Jack Ziegler and was finished with help from Vaughan Thomas, Rémy Mével, Jason Damazo, and Joseph Shepherd.

[2] http://www.galcit.caltech.edu/EDL/public/cantera/doc/tex/ShockDetonation/ShockDetonation.pdf

specific heat at low temperature is given by the following equation

$$\frac{c_p}{R} = \sum_{n=0}^{4} a_n T^n \ .$$ (H.1)

In this case we take the available fits and create new ones without discontinuities. The first step is to select the species whose polynomials require refitting and generating a data set based on the original fits. A choice has to be made about the step size in which to create the data set, which creates stable final polynomials. In this case data has been generated every 100 K and at the mid point the average of the high and low temperature is taken. Then a constrained least squares fitting of the data is performed while keeping the enthalpy of formation and formation entropy the same.

The new fit must maintain the original values of the enthalpy of formation, $\Delta_f h^\circ$, and the formation entropy, $s_\circ(T^\circ)$. Both of these quantities can be computed from the original data. The enthalpy is computed using the first 6 coefficients using the following equation

$$\frac{h}{RT} = \sum_{n=0}^{4} \frac{a_n T^n}{n+1} + \frac{a_5}{T} \ ,$$ (H.2)

where

$$a_5 = \frac{\Delta_f h^\circ}{R} - \sum_{n=0}^{4} \frac{a_n}{n+1} (T^\circ)^{n+1} \ .$$ (H.3)

Thus to maintain the original values of $\Delta_f h^\circ$, it is computed from the initial data and we solve the following equation for the first five constants in the least squares fitting using

$$\left[\frac{h}{RT} - \frac{\Delta_f h^\circ}{RT} \right]_{\text{org}} = \sum_{n=0}^{4} \frac{a_n}{n+1} \left[T^n - \frac{(T^\circ)^{n+1}}{T} \right]$$ (H.4)

and then Equation H.3 for a_5.

The entropy is computed from Equations H.5 and H.6.

$$\frac{s_\circ}{R} = a_0 \ln(T) + \sum_{n=1}^{4} \frac{a_n T^n}{n} + a_6$$ (H.5)

$$a_6 = \frac{s_\circ(T^\circ)}{R} - \left(a_0 \ln(T^\circ) + \sum_{n=1}^{4} \frac{a_n (T^\circ)^n}{n} \right)$$ (H.6)

Similarly, to maintain the original value of $s_\circ(T^\circ)$, it is computed from the original data and we solve Equation H.7 in the least squares fitting

$$\left[\frac{s_\circ}{R} - \frac{s_\circ\left(T^\circ\right)}{R}\right]_{\text{org}} = a_0 \ln\left(\frac{T}{T^\circ}\right) + \sum_{n=1}^{4} \frac{a_n\left(T^n - \left(T^\circ\right)^n\right)}{n} , \tag{H.7}$$

and then solve for a_6 using Equation H.6.

The constrained least squares fitting was carried out with the following constraints applied for the two polynomials:

1. Match lowest and highest value of c_p/R

2. C^0 (continuous) c_p/R at mid point

3. C^1 (1st derivative continuous) c_p/R at mid point

4. Match lowest and highest value of $h/(RT)$

5. C^0 (continuous) $h/(RT)$ at mid point

6. C^0 (continuous $s_\circ/R$ at mid point.

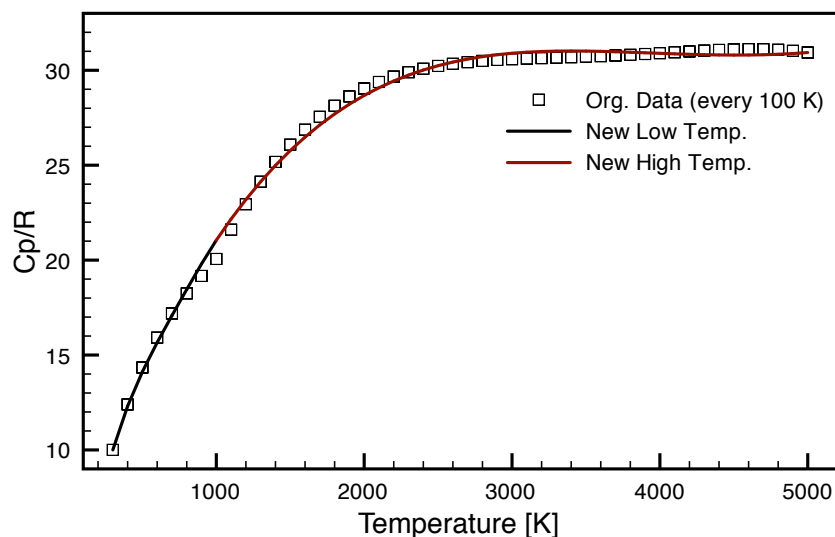The final result of the fitting in Figure H.2 shows the successful refit of the specific heat.

Figure H.2: New thermodynamic data - c_p/R for $C_2H_5CO_2$

In our current version the refitting is performed using MATLAB using the constrained linear least-squares solver `lsqlin` (MATLAB, 2010). The function solves the matrix equation $Ax = b$ using a minimization subject to the constraint equation $A_{eq}x = b_{eq}$. The `lsqlin` function is called in the following way:

```
[x] = lsqlin(A, b, [ ], [ ], Aeq, beq, lb, ub, x0)
```

During the first iteration the starting point is empty, `x0 = [ ]`. The least squares fitting is then called an additional 50 times in a loop using the previous result as the initial condition for the current iteration. The lower and upper bounds, `lb` and `ub`, are simply set at -Inf and +Inf.

The least square equation is set up such that x vector contains the new coefficients for the low temperature, a_n, and high temperature, b_n,

$$x = [a_0, a_1, \cdots, a_5, a_6, b_0, b_1, \cdots, b_5, b_6] \ . \tag{H.8}$$

The A matrix is arranged in the following way:

$$A = \begin{bmatrix} c_p/R \text{ in the low temperature range (M rows)} \\ c_p/R \text{ in the high temperature range (N rows)} \\ h/(RT) \text{ in the low temperature range (M rows)} \\ h/(RT) \text{ in the high temperature range (N rows)} \\ s_\circ/R \text{ in the low temperature range (M rows)} \\ s_\circ/R \text{ in the high temperature range (N rows)} \end{bmatrix}, \tag{H.9}$$

where M is the number of elements in a vector spanning from the lowest temperature to the mid temperature in increments of 100 K, and N s the number of elements in a vector spanning from the mid temperature to the highest temperature in increments of 100 K.

For example, for the specific heat $Ax = b$ is

$$
\begin{bmatrix}
T_1^0 & T_1^1 & \cdots & T_1^4 & 0 & 0 & 0 & 0 & \cdots & 0 & 0 & 0 \\
\vdots & & & & & & & & & & & \\
T_{\text{mid}}^0 & T_{\text{mid}}^1 & \cdots & T_{\text{mid}}^4 & 0 & 0 & 0 & 0 & \cdots & 0 & 0 & 0 \\
0 & 0 & \cdots & 0 & 0 & 0 & T_{\text{mid}}^0 & T_{\text{mid}}^1 & \cdots & T_{\text{mid}}^4 & 0 & 0 \\
\vdots & & & & & & & & & & & \\
0 & 0 & \cdots & 0 & 0 & 0 & T_{\text{max}}^0 & T_{\text{max}}^1 & \cdots & T_{\text{max}}^4 & 0 & 0
\end{bmatrix}
\begin{bmatrix}
a_0 \\ a_1 \\ \vdots \\ a_4 \\ a_5 \\ a_6 \\ b_1 \\ b_2 \\ \vdots \\ b_4 \\ b_5 \\ b_6
\end{bmatrix}
=
\begin{bmatrix}
\frac{c_p}{R}\big|_{\text{org @ } T_1} \\ \vdots \\ \frac{c_p}{R}\big|_{\text{org @ } T_{\text{mid}}} \\ \frac{c_p}{R}\big|_{\text{org @ } T_{\text{mid}}} \\ \vdots \\ \frac{c_p}{R}\big|_{\text{org @ } T_{\text{max}}}
\end{bmatrix}
.
$$

$$(\text{H.10})$$

For the enthalpy and entropy equation the entries of b are the left-hand sides of Equations H.4 and H.7, respectively, computed from the original data.

The constrain equations are implemented in a similar way. For example, matching the specific heat at the mid point is constraint by the following equation:

$$
\begin{bmatrix}
T_{\text{mid}}^1 & T_{\text{mid}}^2 & \cdots & T_{\text{mid}}^4 & 0 & 0 & -T_{\text{mid}}^1 & -T_{\text{mid}}^2 & \cdots & -T_{\text{mid}}^4 & 0 & 0
\end{bmatrix}
\begin{bmatrix}
a_0 \\ \vdots \\ b_6
\end{bmatrix}
= 0 \, . \quad (\text{H.11})
$$

The final step is to compute the remaining error in the fit at the mid point, which in our example is 1×10^{-14} and thus sufficient for the solver. If the error is too large more iterations of the least square fitting should be performed.

This page intentionally left blank.